Sensors and Actuators B 190 (2014) 634–644

Contents lists available at ScienceDirect

Sensors and Actuators B: Chemical

journal homepage: www.elsevier.com/locate/snb

# Thiolene and SIFEL-based microfluidic platforms for liquid–liquid extraction

Sachit Goyal[a,1], Amit V. Desai[a,1], Robert W. Lewis[a,b], David R. Ranganathan[c], Hairong Li[c], Dexing Zeng[c], David E. Reichert[c], Paul J.A. Kenis[a,*]

[a] Department of Chemical & Biomolecular Engineering, University of Illinois, Urbana-Champaign, Urbana, IL 61801, USA
[b] Chemical and Biological Engineering, The University of Sheffield, Sheffield, United Kingdom
[c] Radiological Sciences Division, Mallinckrodt Institute of Radiology, Washington University School of Medicine, St. Louis, MO 63110, USA

ARTICLE INFO

*Article history:*
Received 15 June 2013
Received in revised form 27 August 2013
Accepted 12 September 2013
Available online 20 September 2013

*Keywords:*
Parallel-flow microfluidic platform
Two-phase flow
Organic solvent compatibility
Functionalization of microchannels
Lipophilicity of drugs
Extraction of radiometals

ABSTRACT

Microfluidic platforms provide several advantages for liquid–liquid extraction (LLE) processes over conventional methods, for example with respect to lower consumption of solvents and enhanced extraction efficiencies due to the inherent shorter diffusional distances. Here, we report the development of polymer-based parallel-flow microfluidic platforms for LLE. To date, parallel-flow microfluidic platforms have predominantly been made out of silicon or glass due to their compatibility with most organic solvents used for LLE. Fabrication of silicon and glass-based LLE platforms typically requires extensive use of photolithography, plasma or laser-based etching, high temperature (anodic) bonding, and/or wet etching with KOH or HF solutions. In contrast, polymeric microfluidic platforms can be fabricated using less involved processes, typically photolithography in combination with replica molding, hot embossing, and/or bonding at much lower temperatures. Here we report the fabrication and testing of microfluidic LLE platforms comprised of thiolene or a perfluoropolyether-based material, SIFEL, where the choice of materials was mainly guided by the need for solvent compatibility and fabrication amenability. Suitable designs for polymer-based LLE platforms that maximize extraction efficiencies within the constraints of the fabrication methods and feasible operational conditions were obtained using analytical modeling. To optimize the performance of the polymer-based LLE platforms, we systematically studied the effect of surface functionalization and of microstructures on the stability of the liquid–liquid interface and on the ability to separate the phases. As demonstrative examples, we report (i) a thiolene-based platform to determine the lipophilicity of caffeine and (ii) a SIFEL-based platform to extract radioactive copper from an acidic aqueous solution.



## 1. Introduction

Liquid–liquid extraction (LLE), also referred to as solvent extraction or partitioning, is a method for separating chemical entities based on their selective affinities for one of the phases in a two-phase system, typically an aqueous and an organic phase. Due to its attractive characteristics such as versatility and scalability, LLE has been implemented in a variety of applications at industrial scale including metal extraction [1–3] and organic synthesis [4], in various sample pre-treatment processes (e.g., purification of biomolecules [5], ultra-sensitive measurement of analytes [6,7], pesticide analysis [8]), and in analytical applications, e.g., for the determination of the lipophilicity during drug discovery and development [9].

Conventionally LLE is performed in large containers at scales as large as hundreds of liters by agitation of the multiphase mixture followed by gravity-based phase separation and selective removal of one of the two phases [10,11]. Vigorous agitation of the phases is required to (1) shorten the distances that the chemicals need to traverse by diffusion to the aqueous-organic interface; (2) minimize the formation of the depletion and saturation layers on either side of the liquid–liquid interface; and (3) maximize the contact area. This need for agitation of the phases for efficient extraction necessitates the use of large volumes of aqueous and organic phases, which hampers the utility of LLE for applications involving small reagent volumes (<1 mL), such as sample preparation and/or chemical/biochemical analysis of expensive, limitedly available chemicals [12–14], and extraction of molecules occurring in low concentrations [15,16].

To sidestep these limitations and to enable LLE at much smaller scale, various microfluidic platforms comprised of channels with micron-sized dimensions that use only pico- to micro-liters volumes have been developed [11,15,17–34]. The small dimensions

* Corresponding author. Tel.: +1 2172650523.
*E-mail address:* kenis@illinois.edu (P.J.A. Kenis).
[1] These authors equally contributed to the work.

0925-4005/$ – see front matter © 2013 Elsevier B.V. All rights reserved.
http://dx.doi.org/10.1016/j.snb.2013.09.065

minimize the diffusion distances to such an extent that agitation is not needed anymore. In addition, microfluidic platforms provide the benefits of rapid stabilization of the liquid–liquid interface, a large interfacial area to volume ratio, and amenability to automation [11,21]. These microfluidic platforms are also particularly suitable for detailed investigation of extraction processes, e.g., to derive information of the kinetics of a reaction [15].

Microfluidic platforms for LLE have been developed for a wide range of applications, including the separation of metal ions [30,31,35,36] and the purification of DNA [37]. These microfluidic platforms can be broadly classified into two types: (i) droplet-based and (ii) parallel flow. In *droplet-based microfluidic LLE platforms*, droplets of one phase are controllably formed in the other phase by exploiting the interfacial tension between the two phases. Due to the ability to precisely control parameters such as size and velocity during droplet formation [38,39], these microfluidic platforms have been used for LLE applications, such as the study of reaction kinetics during metal extraction [15]. However, in applications that require off-chip analysis or further processing of one or both phases, the phases need to be separated post-extraction, necessitating additional processing steps that are typically performed manually and are time-intensive. One popular approach to separate the phases is to collect the droplets in a larger compartment where droplets of the same phase will coalesce, although this approach is not straightforward for small volumes (<500 μL) and not easily amenable for automation. Various methods including the use of membranes [11], hydrophilic side channels [40], complex geometries to trap droplets of one phase [18,19], and capillary action-assisted side channels [15] have been developed for continuous, automated phase separation with some success, at the cost of having a much more complex microfluidic system, often involving additional channel surface functionalization steps.

In contrast, *parallel flow-based microfluidic LLE platforms* allow for continuous phase separation, hence obviating the need to use additional steps to separate the phases. This separation is achieved because the two phases come together in a common channel, flow in parallel, form a liquid–liquid interface, and exit through their respective outlets at the end of the common channel. Parallel-flow microfluidic LLE platforms have been used for a wide range of applications including metal extraction such as the extraction of cobalt complex from aqueous solution to toluene [25] and sample preparation for analyses, such as the extraction of ephedrine for gas chromatography [41].

To date, microfluidic parallel-flow LLE platforms have been made using materials that are compatible with organic solvents, mainly glass [12,21–23,35,42] and silicon [11,43–45]. However, fabrication with silicon and glass requires the use of expensive, not easily available infrastructure, and hazardous materials [46–48]. These fabrication-related limitations in principle can be addressed by the development of polymeric microfluidic platforms for LLE that can be fabricated using less involved processes and more easily available infrastructure. While photolithography is often still needed to create the desired patterns, subsequent steps typically only involve replica molding, hot embossing, and bonding at much lower temperatures. Although polymeric microfluidic devices comprised of poly(methyl methacrylate) (PMMA) and poly(dimethylsiloxane) (PDMS) have found widespread application in biochemistry and biology research laboratories [49], most polymers used for microfluidic applications are not compatible with organics solvents that are needed for LLE. Various polymeric materials have been explored for microfluidic applications that require compatibility with certain organic solvents, including thiolene [50–52], untreated fluoropolymers [53], photo-curable or thermally curable perfluoropolyether [54–57], polytetrafluoroethlyene or Teflon [58], thermoset polyester [59,60], cyclic olefin copolymer [61], Viton [62], SU-8 [63], parylene [64], polyimide [65], polyvinyl(silazane) [66], and Dyneon™ THV Fluorothermoplastics [67]. However, the majority of these polymers suffer from one or more of the following limitations that would hamper their use for a parallel flow microfluidic LLE platform: (1) incompatibility with a wide range of organic solvents for extended use; (2) complex, tedious, and cost intensive fabrication (e.g., requiring an oxygen-free environment); (3) non-amenability with rapid prototyping; (4) challenges in inter-layer bonding to obtain leak-free devices; and (5) challenges in interfacing of the microfluidic platform with ancillaries. Here, we achieve solvent compatibility and ease of fabrication by developing parallel flow microfluidic LLE platforms out of thiolene, a UV-curable epoxy resin, and SIFEL, a moldable perfluoropolyether.

Along with material considerations, another important factor for the optimal operation of a parallel flow microfluidic LLE platform is maximizing the contact time between the two phases. This contact time is determined by the geometry of the microchannels, interfacial tension between the two phases, and the interaction of the two phases with the microchannel walls. Previously, various strategies have been explored to stabilize the liquid–liquid interface during LLE in parallel flow, including partial surface functionalization [22,24,42,68,69], placement of membranes [20] or microstructures between the phases [17,25,32], and/or the use of surfactants [37]. Surfactants reduce the interfacial tension between the two phases, which stabilizes the liquid–liquid interface, but their use has been shown to affect the extraction kinetics and reduce the extraction rate because of the reduction in the interfacial contact area between the two phases [33]. Micro porous membranes can be placed between the two phases fairly easily, but this drastically reduces the liquid–liquid interfacial area, and increases the distance across which the chemical species have to diffuse. Partial surface functionalization and the use of microstructures such as posts at the interface has been used successfully to pin the two phases in different parts of the microchannel.

Here we will build on this prior work through a systematic study regarding the effect of surface functionalization and the effect of microstructures on the stability of the liquid–liquid interface and on phase separation in microfluidic LLE platforms. To capture the various physical phenomena of importance to LLE, we developed an analytical model to guide the design of these platforms with the objective of optimizing the extraction efficiency, and to validate the experimental observations. As demonstrative examples of parallel-flow LLE using a microfluidic approach, we report (i) a thiolene-based platform to determine the lipophilicity of caffeine, and (ii) a SIFEL-based platform to extract and purify radioactive copper from an acidic aqueous solution as found in target processing of cyclotron-generated copper-64.

## 2. Materials and methods

Detailed information regarding the materials and the experimental procedures used for the determination of contact angles, the functionalization of microchannel surfaces, the study of interface stability and phase separation, the determination of lipophilicity of caffeine, and the extraction of radioactive copper are provided in the supplementary information.

### 2.1. Fabrication of the thiolene-based microfluidic platform

Fig. 1 provides an overview of the fabrication steps employed to create the thiolene-based microfluidic platform. Negative images of the microchannels, inlets, and outlets of multiple microfluidic platforms were printed on a transparency sheet using a 5080-dpi printer (Pageworks, Cambridge, MA). Patterns of the microfluidic platforms were transferred to an approximately 15 μm thick layer

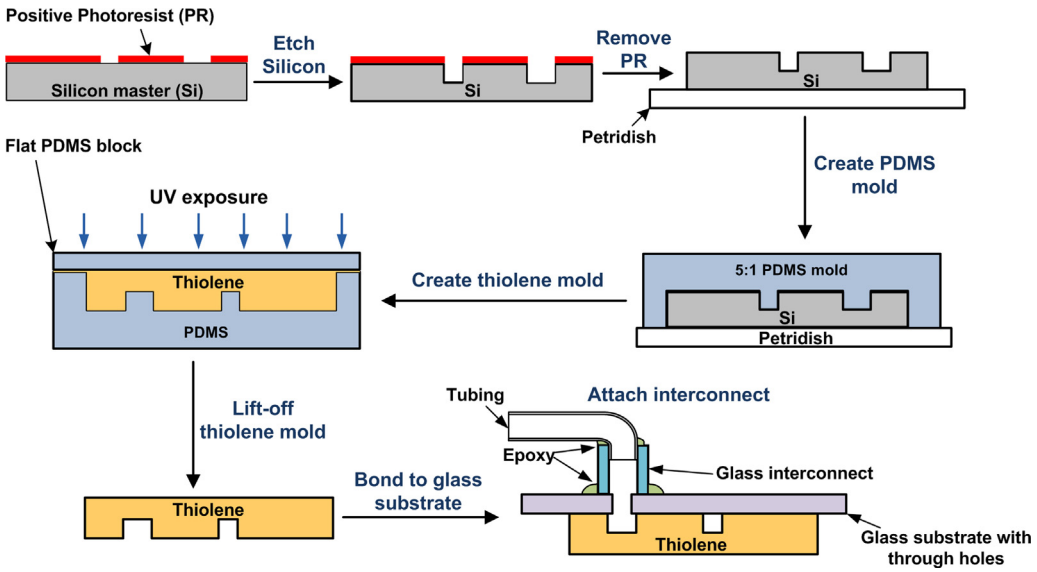


**Fig. 1.** Fabrication steps for the thiolene-based LLX microfluidic platform. The microfluidic platform pattern is created on a silicon wafer by photolithography and deep reactive ion etching (DRIE), followed by replica-molding to obtain a PDMS mold of the microfluidic platform. This PDMS mold is then used to transfer the pattern of microchannels in thiolene by pouring the liquid pre-polymer and subsequent partial curing via UV exposure. The thiolene mold is then brought in contact with a glass substrate with pre-drilled holes at the inlets and outlets of the microchannels and bonded to the glass by prolonged UV exposure. The glass interconnects and PTFE tubing is then bonded at the inlets and outlets by application of epoxy and subsequent room temperature curing.

of SPR 220-7 (Rohm and Haas Electronic Materials) spun onto a 4″ silicon wafer (using G3P-8 Spin Coat by Specialty Coating Systems) by UV photolithography and development in AZ 421K. Next, the microchannels, approximately 50 μm tall, were etched in the wafer by deep reactive ion etching (DRIE, PlasmaTherm ICP-DRIE etching system) for approximately 30 min. Next, the photoresist was washed away with acetone and isopropyl alcohol, and the residual impurities on the wafer were removed by oxygen plasma (RIE, March Jupiter III). The etch depth was confirmed to be within 10% of the intended dimensions using profilometry (KLA Alphastep IQ). The exposed silicon surface was passivated by vapor deposition of (tridecafluoro-1,1,2,2-tetrahydrooctyl) trichlorosilane under vacuum. All the microfluidic platforms were then diced from the 4″ wafer using a diamond scriber (MTI corporation). Next, a PDMS replica of each microfluidic platform was prepared by pouring 5:1 A:B (monomer: cross linker) PDMS on the silicon master placed on a plastic petri dish followed by thermal curing in a convection oven (Thermo Scientific) at 65 °C for 1–2 h. Then, PDMS mold with the embossed features was removed from the silicon master using a scalpel. Liquid thiolene, NOA 81 was poured on the mold and capped by another PDMS block on top, followed by partial curing via UV exposure for 30–40 s. Holes were drilled into a glass substrate (Dremel 300 series drill with a 750 μm McMaster-Carr diamond drill bit) corresponding to the inlets and outlets of the microfluidic platform. The thiolene device was then bonded to the glass slide with pre-drilled holes using further UV exposure for approximately 6 min. The high gas permeability of PDMS and the inhibition of the free radical polymerization induced via UV exposure used to cure thiolene, in the presence of oxygen, ensured that a thin superficial layer of liquid thiolene remains uncured. This resulting film retains adhesive capabilities and enables bonding of thiolene to glass on further UV exposure. Solutions are introduced to and removed from the chip using PTFE tubing (30 AWG, Cole Parmer) that are connected to the chip via glass interconnects. These glass interconnects (ID ~ 0.7 mm, OD ~ 2 mm) were glued to the holes on the glass side using super glue (Loctite™) for temporary bonding followed by application of epoxy glue (Loctite™ Epoxy Quick Set) for permanent sealing. Subsequently, the PTFE tubing was inserted into the glass interconnects and fixed in place by applying the same epoxy glue.

### 2.2. Fabrication of the SIFEL-based microfluidic platform

Fig. 2 provides an overview of the fabrication steps employed to create the SIFEL-based microfluidic platform. Negative images of the microchannels, inlets, and outlets were printed on a transparency film using a 5080 dpi printer. The patterns were transferred to an approximately 50 μm thick layer of photoresist (MicroChem SU-8 2050) spun on a 3″ silicon wafer (University wafer) using standard UV photolithography. The exposed silicon surface was passivated by applying a monolayer of 3M™ Novec™ EGC 1700 Electronic Coating diluted with 3M™ Novec™ DL 7100 Engineering Fluid in ratio 1:4 using a spin-coater at 1500 rpm (G3P-8 Spin Coat by Specialty Coating Systems). This coating prevented covalent adhesion of SIFEL to the silicon substrates and the photoresist. The thicknesses of photoresist and SIFEL layers were verified to be within 10% of the intended dimensions using a surface profilometer (Dektak 3030). The SIFEL replica of the microchannels was prepared by spin coating 1:1.5 A:B (monomer: cross linker) SIFEL at 700 rpm followed by partial thermal curing on a digital hot plate (Dataplate® 730 series, Barnstead Thermolyne) at 110 °C for 7 min. Next, a thin layer (~5 μm) of 15:1 A:B PDMS was spin coated at 3500 rpm and thermally cured at 110 °C. Subsequently, a 4 mil (100 μm) cyclic olefin copolymer (COC) sheet with predrilled holes (Dremel 300 series drill with a 750 μm McMaster-Carr drill bit) corresponding to the inlets and the outlets of the microfluidic platform, was bonded irreversibly to the top of the PDMS-SIFEL layer after 1 min plasma treatment of both components with a plasma cleaner (Harrick; Settings: RF level “Hi”, and pressure of 500–1000 mTorr). The COC-PDMS-SIFEL assembly was then heated at 110 °C for one hour on a hot plate to complete curing. Next, glass interconnects (ID ~ 0.7 mm, OD ~ 2 mm) were glued to the inlets and outlets of the microfluidic platform using super glue (Loctite™) for temporary adhesion followed by application of an epoxy glue (Devcon® 2 ton epoxy) for permanent sealing. The assembly was allowed to cure for 2–3 h at room temperature. Teflon tubing was

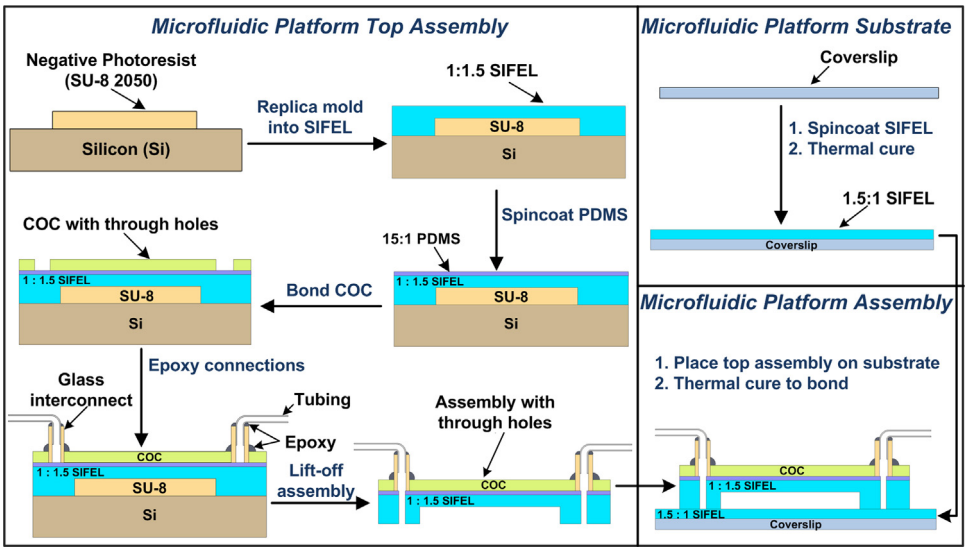


**Fig. 2.** Fabrication steps for the SIFEL-based LLX microfluidic platform. Negative pattern for the microfluidic platform is created on a silicon wafer by photolithography, which is replicated in SIFEL via soft lithography followed by partial curing. A thin layer of PDMS is then spin-coated on top of the SIFEL layer. A cyclic olefin copolymer (COC) sheet with predrilled holes at the inlets and outlets of the microchannels is irreversibly bonded (plasma) to the top of the PDMS-SIFEL layer. The glass interconnects and PTFE tubing is then bonded at the inlets and outlets by application of epoxy and subsequent room temperature curing. Simultaneously, SIFEL is spin coated on a cover slip and partially cured. Finally, the COC-PDMS-SIFEL assembly is lifted off the master and brought in contact with the cover slip spin coated with SIFEL, followed by thermal curing to irreversibly bond the two layers.

then inserted into the glass interconnects and fixed in place using the same epoxy, followed by curing for 2–3 h at room temperature. The whole assembly was then lifted off the silicon wafer. Holes were punched (27G1¼″ Precision Glide® Needle B-D) at the inlets and outlets of the microfluidic platform from the SIFEL side. Simultaneously, the substrate layer was prepared by spin coating 1.5:1 A:B SIFEL at 1500 rpm onto a 24 mm × 60 mm cover slip (Fischerfinest Premium Superslip™) and partial thermal curing on a hot plate at 110 °C for 10–15 min. The COC-PDMS-SIFEL assembly with interconnects was irreversibly bonded to the SIFEL-glass substrate layer by thermal curing at 120 °C to complete fabrication of the SIFEL-based microfluidic platform.

## 3. Results and discussion

### 3.1. Design of the microfluidic platform for LLE

In the design of a microfluidic LLE platform, several geometrical and operational parameters need to be considered simultaneously for optimal performance. Three key requirements for optimal performance are: (1) parallel co-flow of the liquid–liquid interface along the length of the microchannel; (2) clean phase separation at the exit, i.e., minimal mixing of the phases at the exit; and (3) high extraction efficiency. We designed our microfluidic LLE platform to be double Y-shaped (Fig. 3(a)). The angle between the inlet channels (and outlet channels) was designed to be 56° based on a previous study [24], as it allows for phases to come in contact at the inlet with minimal turbulence and a clean separation of the phases at the end. The stability of the liquid–liquid interface depends on the length of the microchannel, because the interface becomes unstable beyond a certain length leading to undesired segmented (slug) flow. Although this requirement of having a stable liquid–liquid interface can be achieved by using shorter channel lengths, shorter microchannels will reduce the extraction efficiency due to the shorter contact times. The extraction efficiency and the stability of the interface also depend on the cross-sectional dimensions of the microchannels. Hence, for optimal design of the microfluidic LLE platform, we derived two analytical expressions, one to predict the maximum extraction efficiency and one to predict the maximum length for which the interface is stable.

First, we derived an expression for the maximum length over which the liquid–liquid interface is stable before breaking up in droplets (Eq. (1)). We will call this length the *maximum extraction length*, $L_{ext}$, which depends on the balance between the hydrodynamic viscous forces and the interfacial surface tension forces at the liquid–liquid interface (Fig. 3(b)). The expression for the maximum extraction length is derived using the generic expression for the hydrodynamic resistance and hence, is valid for microchannels

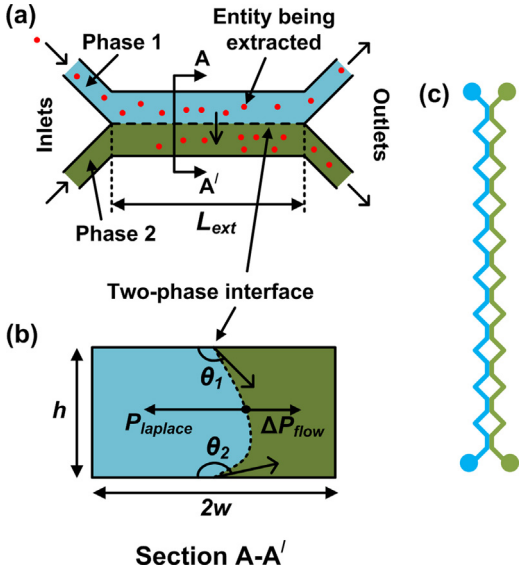


**Fig. 3.** (a) Schematic illustration of a parallel-flow microfluidic platform, where a chemical entity (shown in red) is being extracted from Phase 1 to Phase 2. (b) Cross-sectional view of the microfluidic platform, showing the balance between hydrodynamic viscous pressures ($\Delta P_{flow}$) and Laplace pressure ($P_{laplace}$), resulting from surface tension. The contact angles ($\theta_1$ and $\theta_2$) will be not be the same for different surfaces. (c) A split-length design for a LLX microreactor, comprising 10 extraction segments. (For interpretation of the references to color in this figure legend, the reader is referred to the web version of the article.)

with any cross-sectional shape, whereas similar expressions reported previously only applied to rectangular channels [32–34].

Second, we derived an expression to predict the *maximum extraction efficiency*, $\Psi$, by assuming that the rate-limiting step during the extraction process is determined by the rate of diffusion transverse to the direction of flow (Eq. (2)). The value of extraction efficiency predicted by Eq. (2) will typically be an upper limit, because certain additional factors that were ignored due to assumptions in the derivation of Eq. (2), may very well reduce the extraction performance. For example, in reality the rate of extraction at the interface is typically finite, yet was assumed to be infinite (to obtain tractable equations), which may slow down the extraction process. Details of the derivation of Eqs. (1) and (2) are provided in Sections 7 and 8 of the supplementary information.

$$L_{\text{ext}} = \frac{(2\gamma \sin(\theta_{\text{contact}} - 90))/h - \Delta P_{\text{outlet}}}{Q_{\text{aq}} R_{\text{aq-ext}} - Q_{\text{org}} R_{\text{org-ext}}}, \quad (1)$$

$$\Psi = 1 - \left[ \frac{1}{L_{\text{ext}} w} \int_0^{L_{\text{ext}}} \int_0^{w} \sum_{n=1,3,5,\ldots} \exp^{-\lambda_n^2 k^2 z} \sin\left(\frac{n\pi}{2} x\right) dx dz \right], \quad (2)$$

where $L_{\text{ext}}$ is the maximum extraction length of the microchannel; $\gamma$ is the surface tension between the two phases; $\theta_{\text{contact}}$ is the contact angle between the two phases; $w$ is the half-width of microchannel; $h$ is the height of microchannel; $\Delta P_{\text{outlet}}$ is the difference between the hydrodynamic pressures in the outlets; $Q_{\text{aq}}$ and $Q_{\text{org}}$ are the flow rates of the aqueous and organic phases, respectively; $R_{\text{aq-ext}}$ and $R_{\text{org-ext}}$ are the hydrodynamic resistance of the microchannel per unit length in the extraction zone of the aqueous and organic phases, respectively; $\Psi$ is the maximum extraction efficiency; $D_{\text{ext}}$ is the diffusivity of the extracting species; $U_{ext}$ is the linear velocity of the phase in which the extracting species is diffusing toward the interface

$$k = \sqrt{\frac{D_{\text{ext}}}{U_{\text{ext}}}} \quad \text{and} \quad \lambda_n = \frac{n\pi}{2w}.$$

Eqs. (1) and (2) can be used to optimize the design of the microfluidic LLE platform within the constraints of application requirements (e.g., desired extraction efficiency) and fabrication limitations (e.g., minimum feature size). As an example, Fig. 4 shows contour plots, also referred to as design maps, for $L_{\text{ext}}$ (Fig. 4(a)) and $\Psi$ (Fig. 4(b)), for developing a microfluidic platform to extract copper in a water–toluene system (one of the applications discussed later) using microchannels of different dimensions and operated at different flow rates. The details of the parameters used for generating the plots are described in Section 9 of the supplementary information.

Fig. 4(a) shows that larger channel widths enable the use of a wider range of flow rates. The reason the channel width influences the range of allowable flow rates is that high operating backpressures, which can occur in lower width channels, can destabilize the interface by exceeding the Laplace pressure. Fig. 4(b) shows that a combination of higher flow rates and larger channel widths lead to lower extraction efficiencies. Although the extraction efficiency can be increased by decreasing the flow rate (increased contact time), a lower limit to the flow rate is imposed by the interfacial or Laplace pressure [33], which again has to be balanced by the hydrodynamic flow pressure to avoid breakup of the parallel flow pattern into a segmented flow. Alternatively, the contact time can be increased by increasing the length of the microchannel, but as explained above, this length has a maximum as determined by Eq. (1). To avoid the parallel flow pattern breaking up by using a flow rate that is too low or by using a channel that is too long, a split-length design (Fig. 3(c)) can be used, in which the length of the individual segments is smaller than the maximum extraction

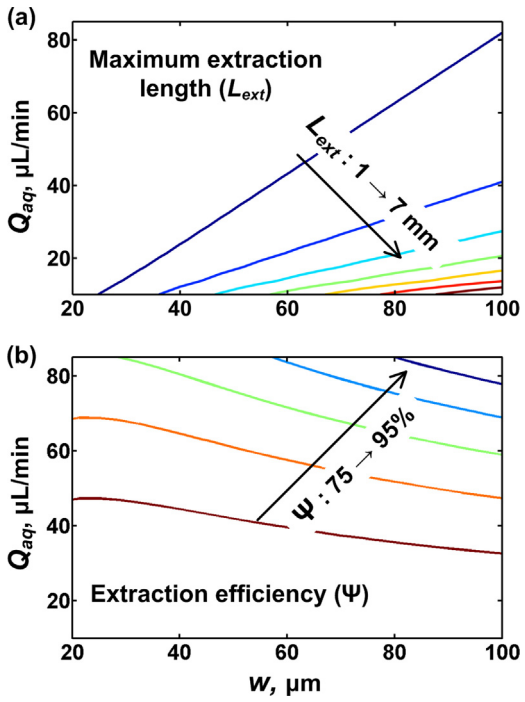


**Fig. 4.** Design maps showing contour plots for (a) maximum extraction length, $L_{\text{ext}}$, and (b) extraction efficiency length, $\Psi$, as a function of microchannel half-width ($w$) and aqueous flow rate ($Q_{\text{aq}}$). The contour lines for extraction length vary from 1 to 7 mm in increments of 1 mm, while the lines for efficiency vary from 75% to 95% in increments of 5%.

length. Previously, silicon- and glass-based microfluidic configurations have been reported for parallel flow extraction that use microstructures, including posts, micro pillars, or partitions at the interface to stabilize the liquid–liquid interface [17,32]. Although these strategies were effective in stabilizing the liquid–liquid interface, these structures effectively reduced the extraction length, and these platforms contain features with smaller than 5 μm dimensions, which generally are more challenging to fabricate than the ~100 μm channels used in the split-length design studied here, especially in certain materials such as flexible polymers [70].

The gap between the microstructures and the size of the microstructures determine the contact time, and the time during which the two phases are not in contact with each other. The throughput of the split-length design is comparable or higher than those of previous platforms [17,32]. In prior platforms, integration of microstructures at the liquid–liquid interface typically reduces the contact area by at least 50%, more typically by 75+% [17,32]. In the specific split-length design used in this study, the liquid–liquid interfacial area has been reduced by 50%, but the segments that separate the individual contact areas in principle can be reduced in size so that the liquid–liquid interfacial area is reduced by 25% less. We used Eqs. (1) and (2) to predict optimal microchannel dimensions and operating parameters for the microfluidic LLE platforms and we experimentally tested interface stability and phase separation for different microfluidic platforms (see Section 3.3).

### 3.2. Material choice for microfluidic LLE platforms

Thiolene and SIFEL were chosen on the basis of their excellent resistance to a wide range of organic solvents, including hexanes, toluene, and n-octanol, and minimally swell on prolonged exposure [56,57,71]. Particularly, SIFEL was also chosen due to its inert nature [57]. Both materials have been used previously for microfluidic applications, although using different fabrication procedures than presented here, to develop organic

solvent-compatible microfluidic platforms [50,52,56,57,71,72]. A few examples have been reported where SIFEL or thiolene based microfluidic chips have been used for applications involving multiphase flow [56,71–73]. Here, we demonstrate the application of these materials for parallel-flow microfluidic LLE platforms by co-flowing immiscible phases together, which has not been exploited with polymer-based microfluidic platforms to date.

Thiolene and SIFEL-based microfluidic platforms can be fabricated via replica molding from a master pattern, which makes the fabrication process amenable for rapid prototyping. We fabricated the thiolene-based microfluidic platform by first etching a pattern into a silicon wafer to obtain a primary master that are then replicated in PDMS molds with very smooth surfaces. (Creating identical primary masters via patterning of photoresist does not provide the required, less than 1 μm variation in flatness of the surfaces.) These PDMS molds then served as the master for the creation of the thiolene-based platforms via replica molding. Both the primary silicon master and the PDMS replica can be used repeatedly so multiple thiolene replicas can be obtained rapidly. While creation of the thiolene structures required a very flat master, the SIFEL structures could be obtained by direct replication of a photoresist based master. Complete thiolene-based microfluidic platforms were obtained by bonding the thiolene replica against a glass slide by UV exposure. SIFEL-based microfluidic platforms were obtained by thermal curing of a SIFEL replica against a SIFEL-covered glass slide. Next interconnects were mounted on the inlets and outlets. Then, we exposed these microfluidic platforms to organic solvents for prolonged duration (at least 2 h) to confirm leak-free operation. The platforms exhibited minimal or no swelling upon exposure to solvents such as octanol and toluene which further ensured the compatibility of the SIFEL- and thiolene-based platforms with the organic solvents of interest.

### 3.3. Interface stability and quality of phase separation

Since stability of the liquid–liquid interface (i.e., no droplet formation) and ideal phase separation (i.e., no mixing of the phases at the exit) are critical for the operation of parallel-flow microfluidic LLE platforms, we initially tested them for these two phenomena. Based on the analytical model, we first designed a microfluidic platform, comprised of a single, short channel, with an extraction length ($L_{ext}$) of 4 mm, a channel height ($h$) of 50 μm, and a channel width ($2w$) of 200 μm (i.e., half channel width "$w$" = 100 μm in Fig. 4). We chose $L_{ext}$ to be 4 mm as the value is an intermediate value between the minimum and maximum values for extraction lengths that we estimated from the design maps (Fig. 4(a)). For the channel width, we picked the maximum value in the design map, because a larger width enables the use of a wider range of flow rates, which in turn provides more flexibility to achieve optimal extraction efficiency. A channel height of 50 μm was chosen, which is larger than the channel heights used in previously reported silicon and glass parallel-flow LLE platforms [12,16,17,22,41]. According to the model larger heights can be chosen, which is advantageous as it increases the area of the liquid–liquid interface.

Initial testing for interface stability and quality of the phase separation was performed with *the thiolene-based microfluidic platforms* (experimental details in Section 4 of the supplementary information). As predicted by the analytical model (Eq. (1)), we observed a stable liquid–liquid interface when water–toluene and water–octanol systems were used. Obtaining a stable liquid–liquid interface in a short, 4-mm long channel is advantageous compared to other methods used for stabilization of the liquid–liquid interface that use microstructures [17,32], membranes [11,28], or surfactants [37], with respect to fabrication amenability and versatility. As explained above, the need to balance the hydrodynamic and surface tension forces (Fig. 3(b)) to ensure parallel flow imposes a constraint on the channel length (see design maps, Fig. 4(a)). To achieve the larger liquid–liquid interfacial area needed to achieve the desired level extraction, multiple short channels can be arranged in series by using the split-length design (Fig. 3(c)), introduced in Section 3.1.

Although we observed a stable, parallel two-phase interface along the length of the microchannel, separation of the phases into the two outlet channels was not ideal, i.e., one of the phases leaked into the other at the exit. This phenomenon can be attributed to preferential wetting of the microchannel surfaces by one of the phases, resulting in leaking of that phase into the outlet of the other phase. For example, in the case of the thiolene-based microfluidic platform, all surfaces of the microchannels, both thiolene and glass, are hydrophilic, so water tends to leak into the outlet of the toluene phase. Previously, this issue has been overcome for glass-based microfluidic platforms via partial functionalization of the microchannels with a hydrophobic coating, such that both phases are guided into their respective outlets due to preferential wetting of the treated, hydrophobic surfaces by the organic phase [12,30,41,69]. Based on these studies, we applied a hydrophobic surface coating to the fraction of the microchannel surface that is exposed to the organic phase by flowing isooctane containing 1 wt.% of (heptadecafluoro-1,1,2,2-tetrahydrodecyl)trichlorosilane or FDTS (a silane reagent for functionalizing the surface of thiolene [72]) in parallel laminar flow with isooctane (experimental details: Section 2 of the supplementary information). This partial surface modification improved the phase separation as evidenced by the presence of significantly lower quantity of aqueous phase in the collected organic phase. To further improve the phase separation, we performed the same surface functionalization protocol in the reverse direction, by introducing the FDTS solution from the outlet. This eliminates the possibility for the pure octane and the octane with silane to mix before reaching the outlet sections, where the precision of surface patterning is crucial.

To confirm that the surfaces were functionalized to be hydrophobic, we performed two-phase contact angle measurements on untreated and on silane-treated thiolene and glass substrates (experimental details: Section 3 of the supplementary information). The contact angle of a droplet of toluene submerged in water changed from approximately 65° and 88° for untreated glass and thiolene, respectively, to approximately 135° for both after silane treatment. Similarly the contact angles changed from approximately 82° and 136° for untreated glass and thiolene, respectively, to approximately 140° for the silane-treated surfaces, when observing a droplet of water submerged in octanol. The treated surfaces exhibited these contact angles changes within 10 min of silane treatment, after which they remained constant even after prolonged silane treatment (i.e., 30 min).

As a control experiment, we also completely functionalized the microchannel surfaces with silane and compared the quality of the phase separation with that obtained in a partially functionalized microfluidic platform. Surprisingly, we observed that full functionalization of the microchannel surfaces resulted in a better phase separation at the outlet in terms of lower leakage of the aqueous phase into the octane phase (vol. of aqueous phase < 5% of total volume of the organic phase) as well as a higher reliability. This observation seems counter-intuitive at first, as fully functionalized microchannels are expected to behave similar to microchannels whose surfaces have not been treated. For the un-functionalized thiolene-based microfluidic platform, however, one of the contacting surfaces is glass and the other is thiolene, each with different wetting properties (Fig. 3(b)), whereas when all surfaces are uniformly functionalized with silane all the surfaces exhibit similar wetting behavior (identical contact angles, see above). These observations were confirmed when studying the quality of the phase separation for the SIFEL-based microfluidic platform, which is

comprised of a SIFEL-covered glass slide and a patterned SIFEL mold, so all surfaces are identical from the onset. Also here good phase separation between water and toluene was observed (<5% leakage of the toluene into the aqueous phase) (Fig. 6(b)). Based on these observations, we conclude that uniform functionalization of all the surfaces is more important for ideal phase separation than the confinement of the two phases by partial functionalization. A more detailed explanation for these observations, which is based on the presence of wettability gradients on the channel surface at the liquid–liquid interface, is provided in the supplementary information.

Another factor that determines the quality of the phase separation is the position of the aqueous-organic interface, which should be close to the central axis of the microchannel for ideal separation. When the aqueous and organic phases used have different viscosities, the relative flow rates need to be adjusted in order to position the interface at the center. The ratio of the two flow rates can be correlated directly to the ratio of the viscosities of the solutions [74]. We were able to position the interface in the center of the channel, and accomplish good phase separation when using flow rates of 10 and 45 μL/min for water and octanol, respectively, and 20 and 35 μL/min for water and toluene, respectively.

When we increased the extraction length from 4 to 10 mm to increase the contact time between the two phases, we observed instabilities along the liquid–liquid interface between the phases, which resulting in a poor phase separation, as predicted by analytical modeling (see above). To still achieve the goal of increased contact time, we used a split-length design comprised of 10 segments of 1 mm length each (Fig. 3(c)), which significantly improved phase separation (Fig. 5(b)). The short extraction length of each section prevents the liquid–liquid interface from becoming unstable. Thus, the split-length design enables extension of the contact time between two phases, while still ensuring a stable liquid–liquid interface and clean phase separation at the exit.

### 3.4. Validation of the parallel flow microfluidic LLE platforms

#### 3.4.1. Determination of lipophilicity of caffeine using thiolene-based microfluidic LLE platform

The attrition of parent compounds (PCs) during the drug development process, for example due to poor *in vivo* physiological properties (e.g., poor pharmacokinetics and toxicity), has resulted in the development of *in vitro* methods that can be used in the early stages of drug development for estimation of PC bioavailability. Specifically, ADME parameters (absorption, distribution, metabolism, and excretion) of a PC are determined early on in the drug discovery process. A PC molecule's lipophilicity is an important ADME parameter that greatly influences the overall PC bioavailability [13]. Traditionally, the lipophilicity of a molecule is estimated by measuring the octanol–water distribution coefficient ($\log D$) of the molecule via liquid–liquid extraction in a shake flask, where $D$ is the ratio of concentration in n-octanol phase to concentration in the aqueous buffer. Log $D$ enables prediction of the passive permeation of a PC molecule through the wall of the gut, and also correlates to the permeability of the blood-brain barrier and the extent to which a PC affects plasma-protein binding [9]. The traditional shake-flask method is simple to operate, but the method is time-intensive and requires significant amounts of PC material (~15 mg) to obtain accurate $\log D$ values. This current method precludes investigation of the lipophilicity of compounds that are only available in small quantities as well as of large libraries of compounds. These issues can be overcome by using microfluidic platforms that require low sample volumes, allow rapid interface stabilization, minimize the use of organic solvents, and enhance the extraction efficiency due to the advantage of high interfacial area and small diffusional lengths. Here, we validated the thiolene-based microfluidic LLE platform for the determination of the lipophilicity of caffeine, a model pharmaceutical compound. The reason for choosing thiolene for lipophilicity assays is that thiolene is compatible with n-octanol, a commonly used organic solvent in these assays.

The extraction experiments were conducted using the split-length design microfluidic platform with 10 mm total length, 200 μm width, and 50 μm height, fully functionalized with 1 wt.% FDTS in iso-octane (Fig. 5(a)). Further experimental details can be found in Section 5 of the supplementary information. The flow rates of the octanol phase (containing 1 mM caffeine) and the phosphate buffer (aqueous phase) that resulted in a stable aqueous-organic interface and a clean phase separation were 10 μL/min and 45 μL/min, respectively (Fig. 5(b)).

Next we performed the caffeine extraction between the octanol solution and phosphate buffer in three consecutive runs each with a contact time of approximately 0.3 s, for a total contact time between the aqueous and the organic phases of 1 s (Fig. 5(c)). The solutions collected at the outlets after the first run where used as the starting solutions for the second run. Similarly, the solution collected at the outlets of run 2, were used for the third run. After every run, a 20-μL aliquot of the solutions at each of the outlets was collected and analyzed using high performance liquid chromatography (HPLC) to determine the caffeine content in both the octanol and the phosphate buffer phase.

We estimated extraction efficiencies of caffeine as a function of contact time until equilibrium was reached (Fig. 5(d)). The mean extraction efficiency from the octanol phase to the aqueous phase after contact times of 0.3 s (1 run), 0.6 s (2 runs), and 0.9 s (3 runs) were observed to be 12%, 34%, and 58%, respectively. We did not observe any improvement in the extraction efficiency after the 3rd run (data not shown), which implied that 58% was the equilibrium extraction efficiency. This equilibrium extraction efficiency yielded a distribution coefficient ($\log D$) value of −0.14, which is in good agreement with the value obtained using the shake-flask method [13]. The microfluidic platform approach required only about 1 mL of the drug solution, thus drastically reducing the amount of PC needed to determine its lipophilicity, compared to the sample quantity needed for a volume of the 50–200 mL required in the shake-flask method. Furthermore, phase separation in the microfluidic setup is achieved by the parallel-flow design, whereas an additional phase separation step based on density is needed in the shake-flask method.

#### 3.4.2. Extraction of radioactive copper using SIFEL-based microfluidic LLE platform

Radioisotopes of metals (e.g., Cu-64 and Y-86) produced using a cyclotron are crucial in nuclear medicine, for example for positron emission tomography (PET) imaging. The production of these isotopes involves the irradiation of a solid target on the cyclotron beam line, followed by dissolution of the target in aqueous acid. The desired isotope is separated from the target material via ion chromatography. As an alternative to this method, we sought to evaluate a microfluidic based LLE process for extracting Cu-64. LLE has been widely utilized with radioisotopes, an example is the UNEX process designed for the large-scale separation of radionuclides found in nuclear waste, is used to isolate radionuclides from the acidic waste solutions [75–77]. However, with a cyclotron target run only micro to milligram quantities of the radioisotope is produced which can be dissolved in a few milliliters of solvent. The development of a microfluidic processing platforms offers (i) the use of low sample volumes, eliminating the need for excessive dilution; (ii) allows rapid interface stabilization; (iii) produces much smaller amounts of organic solvent waste; and (iv) enhances the extraction efficiency of radio metal due to the large interfacial area and small diffusional lengths attained in microfluidic

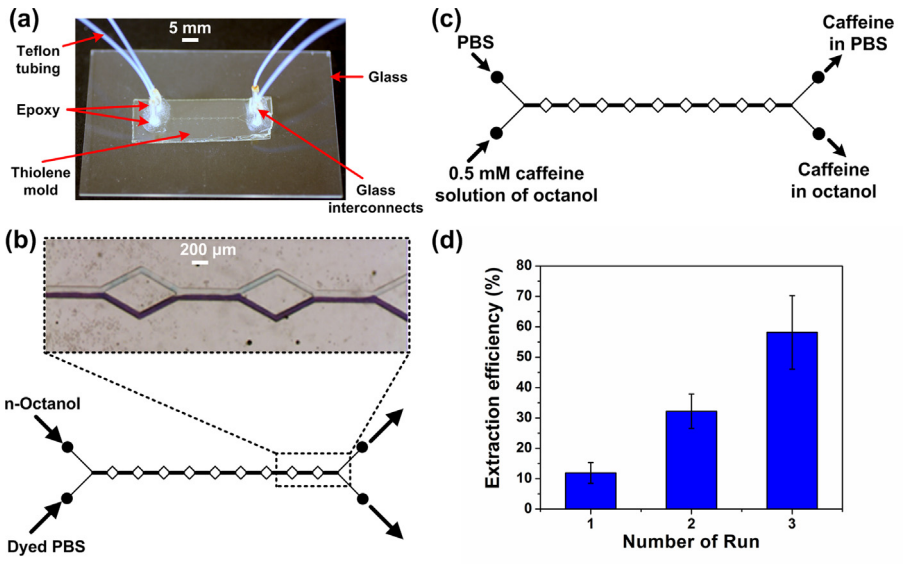


**Fig. 5.** (a) Image of the thiolene-based split-length design microfluidic platform with the various components. (b) Optical micrograph of dyed PBS (aqueous) and octanol (organic) co-flowing in a microchannel fully functionalized with 1% FDTS in iso-octane. The interface was positioned along the centerline and the leakage of the phases at the exit was almost absent. (c) Schematic illustration of the reactor and solutions to study extraction of caffeine from octanol to PBS. (d) Extraction efficiencies of caffeine from octanol to PBS phase as a function of time. Contact time of the two phases during each run was ~0.3 s. Errors bars represent the standard error of the mean (SEM) for 4 experiments.

systems. Here, we demonstrate the application of SIFEL-based microfluidic platform to extract radioactive copper (Cu-64) from an aqueous solution into a toluene solution of 2-hydroxy-4-*n*-octyloxybenzophenone oxime (HOBO), which serves as a chelating agent that selectively binds to Cu-64 metal [78].

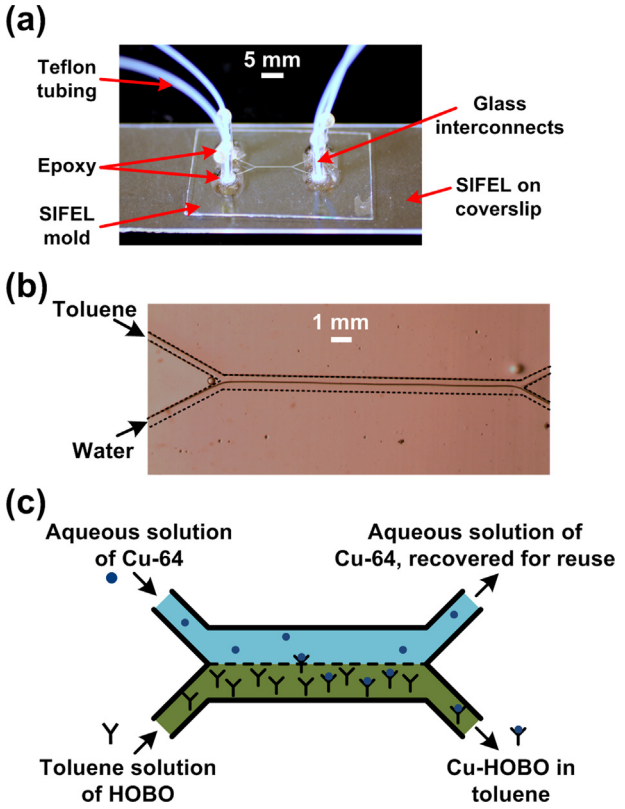


**Fig. 6.** (a) Image of the SIFEL-based microfluidic platform with the various components. (b) Optical micrograph of DI water (aqueous) and toluene (organic) co-flowing in a microchannel. The walls of the microchannels have outlined with dashes for the purpose of clarity. (c) Schematic illustration of the microfluidic platform to study the extraction of Cu-64 from aqueous solution to a toluene solution containing an extracting ligand, HOBO.

The extraction experiments were conducted using a microfluidic platform with a length of 7 mm, and channels that 200 μm wide and 50 μm high (Fig. 6(a)). Further experimental details can be found in Section 5 of the supplementary information. The respective flow rates of the aqueous phase (containing Cu-64 in 0.1 M HCl, pH ~ 5) and the organic phase (containing 10 μM HOBO dissolved in toluene) that ensured a stable liquid–liquid interface and good phase separation at the exit of the microchannel were 20 and 35 μL/min, respectively. At these flow rates the contact time of the aqueous stream was 0.21 s. A stable liquid–liquid and good phase separation could be achieved without functionalization of the channel surfaces (Fig. 6(b)).

We conducted four different experiments, two experiments with a Cu-64 activity of 0.5 mCi/mL and the other two at the concentration of 4 mCi/mL. In each experiment we observed that the radioactive Cu-64 was extracted from the aqueous phase to the organic phase containing HOBO with very high efficiency, often exceeding 95%. These high extraction efficiencies corroborated with estimates from analytical modeling, where we assumed that the extraction is a diffusion-limited process. This assumption is valid for the copper extraction experiments performed here, as the concentration of HOBO is almost six orders of magnitude larger than copper, which leads to extremely fast reaction kinetics, and consequently the extraction is a diffusion-limited process. A more detailed explanation on the validity of this assumption is provided in Section 11 in the supplementary information.

## 4. Conclusions

In this paper, we reported the development of parallel-flow microfluidic platforms for LLE fabricated out of polymeric materials. These microfluidic platforms are made of thiolene and SIFEL, materials that are (1) compatible with a range of organic solvents and (2) amenable to simple, low-temperature, and easily accessible fabrication processes. Comparing the two materials, SIFEL is chemically more inert than thiolene, but more expensive. We developed a generalized analytical model to optimize the design and operation of the microfluidic platform to achieve maximum extraction efficiency while ensuring that the dimensions are within the

limitations of the fabrication methods used. The analytical model can be used to design parallel-flow microfluidic LLE platforms for a variety of applications. We demonstrate for the first time that, as long as the extraction length is less than the analytically predicted maximum value, the separation of the phases is more efficient when the two-phase interface uniformly wets the contacting surfaces (top and bottom surfaces in the configuration reported in the paper). This uniform wetting behavior can be achieved by chemical functionalization of the surfaces of all microchannel walls in the case dissimilar materials are used for their walls.

We validated the thiolene-based microfluidic platform by measuring the lipophilicity of caffeine, and the observed the distribution coefficient was comparable to values obtained in the literature. Similarly, we were able to achieve high extraction efficiencies when using the SIFEL-based microfluidic LLE platform to extract radioactive copper. These high extraction efficiencies were primarily due to the small diffusion lengths (<100 μm), in full agreement with predictions made with the analytical model.

Compared to existing droplet-based polymeric microfluidic LLE platforms that require outlet channels with different wettability to achieve phase separation [15,18,19,40], in the parallel-flow microfluidic LLE designs studied here phase separation can be achieved by splitting the two phases into two identical outlet channels. Furthermore, the polymeric microfluidic platforms can be fabricated using relatively simple, inexpensive methods compared to those used to create similar designs in glass or silicon. One limitation of these polymeric platforms from a fabrication point of view is the need to functionalize the inner walls of the channels in case of a thiolene-glass microfluidic platform; however, this functionalization is also required in microfluidic platforms manufactured out of glass or silicon. Another limitation of these platforms is that counter current flow, which is typically more efficient for extraction compared to co-flow, is challenging to implement due to issues with stabilization of the liquid–liquid interface. These parallel flow polymer-based microfluidic LLE platforms may find use in a wide range of applications, including extraction processes that are constrained by low reagent volumes, sample purification prior to chemical and biochemical analysis, and analytical platforms for the determination of the reaction kinetics (e.g., kinetics of reactive extractions).

## Acknowledgements

Part of this work made use of the facilities in the Frederick Seitz Materials Research Laboratory Central Facilities and Micro-Nano-Mechanical Systems Cleanroom at University of Illinois at Urbana-Champaign, which is partially supported by the U.S. Department of Energy under grants DE-FG02-07ER46453 and DE-FG02-07ER46471. S.G. acknowledges a fellowship from FMC Technologies. We are grateful for the funding support from the Department of Energy Office of Biological and Environmental Research, Grant DEFG02-08ER64682 & DE-SC00002032 (fellowship to D.R.R.) as well as the National Cancer Institute of the National Institutes of Health (Grant CA161348). We also thank the cyclotron facility and staff of the Mallinckrodt Institute of Radiology, Washington University School of Medicine for their support in the production of radioisotopes. We also thank Dr Haiying Zhou for the synthesis of HOBO used in some of these studies.

## Appendix A. Supplementary data

Supplementary material related to this article can be found, in the online version, at http://dx.doi.org/10.1016/j.snb.2013.09.065.

## References

[1] I. Billard, A. Ouadi, C. Gaillard, Liquid–liquid extraction of actinides, lanthanides, and fission products by use of ionic liquids: from discovery to understanding, Analytical and Bioanalytical Chemistry 400 (2011) 1555–1566.
[2] M.L.P. Reddy, T. Prasada Rao, A.D. Damodaran, Liquid–liquid extraction processes for the separation and purification of rare earths, Mineral Processing and Extractive Metallurgy Review 12 (1993) 91–113.
[3] D.M. Roundhill, I.B. Solangi, S. Memon, M.I. Bhanger, M. Yilmaz, The liquid–liquid extraction of toxic metals (Cd, Hg and Pb) by calixarenes, Pakistan Journal of Analytical and Environmental Chemistry 10 (2009) 1–13.
[4] L. Andreani, J.D. Rocha, Use of ionic liquids in biodiesel production: a review, Brazilian Journal of Chemical Engineering 29 (2012) 1–13.
[5] P.G. Mazzola, A.M. Lopes, F.A. Hasmann, A.F. Jozala, T.C.V. Penna, P.O. Magalhaes, C.O. Rangel-Yagui, A. Pessoa Jr., Liquid–liquid extraction of biomolecules: an overview and update of the main techniques, Journal of Chemical Technology & Biotechnology 83 (2008) 143–157.
[6] V. Kuba, Liquid–liquid extraction flow injection analysis, Critical Reviews in Analytical Chemistry 22 (1991) 477–557.
[7] C.I.C. Silvestre, J.L.M. Santos, J.L.F.C. Lima, E.A.G. Zagatto, Liquid–liquid extraction in flow analysis: a critical review, Analytica Chimica Acta 652 (2009) 54–65.
[8] S.C. Cunha, J.O. Fernandes, M.B.P.P. Oliveira, Current trends in liquid–liquid microextraction for analysis of pesticide residues in food and water, in: M. Stoytcheva (Ed.), Pesticides – Strategies for Pesticides Analysis, 2011, pp. 1–27.
[9] F. Lombardo, M.Y. Shalaeva, K.A. Tupper, F. Gao, ElogD$_{oct}$. a tool for lipophilicity determination in drug discovery. 2. Basic and neutral compounds, Journal of Medicinal Chemistry 44 (2001) 2490–2497.
[10] C. Bauer, P. Bauduin, J.F. Dufrêche, T. Zemb, O. Diat, Liquid/liquid metal extraction: phase diagram topology resulting from molecular interactions between extractant, ion, oil and water, The European Physical Journal Special Topics 213 (2012) 225–241.
[11] J.G. Kralj, H.R. Sahoo, K.F. Jensen, Integrated continuous microfluidic liquid–liquid extraction, Lab on a Chip 7 (2007) 256–263.
[12] T. Maruyama, J.-i. Uchida, T. Ohkawa, T. Futami, K. Katayama, K.-i. Nishizawa, K.-i. Sotowa, F. Kubota, N. Kamiya, M. Goto, Enzymatic degradation of p-chlorophenol in a two-phase flow microchannel system, Lab on a Chip 3 (2003) 308–312.
[13] M. Alimuddin, D. Grant, D. Bulloch, N. Lee, M. Peacock, R. Dahl, Determination of log *D* via automated microfluidic liquid–liquid extraction, Journal of Medicinal Chemistry 51 (2008) 5140–5142.
[14] R. Hu, X. Feng, P. Chen, M. Fu, H. Chen, L. Guo, B.-F. Liu, Rapid, highly efficient extraction and purification of membrane proteins using a microfluidic continuous-flow based aqueous two-phase system, Journal of Chromatography A 1218 (2011) 171–177.
[15] K.P. Nichols, R.R. Pompano, L. Li, A.V. Gelis, R.F. Ismagilov, Toward mechanistic understanding of nuclear reprocessing chemistries by quantifying lanthanide solvent extraction kinetics via microfluidics with constant interfacial area and rapid mixing, Journal of the American Chemical Society 133 (2011) 15721–15729.
[16] H. Hotokezaka, M. Tokeshi, M. Harada, T. Kitamori, Y. Ikeda, Development of the innovative nuclide separation system for high-level radioactive waste using microchannel chip – extraction behavior of metal ions from aqueous phase to organic phase in microchannel, Progress in Nuclear Energy 48 (2006) 439–447.
[17] T. Maruyama, T. Kaji, T. Ohkawa, K.-i. Sotowa, H. Matsushita, F. Kubota, N. Kamiya, K. Kusakabe, M. Goto, Intermittent partition walls promote solvent extraction of metal ions in a microfluidic device, Analyst 129 (2004) 1008–1013.
[18] H. Shen, Q. Fang, Z.-L. Fang, A microfluidic chip based sequential injection system with trapped droplet liquid–liquid extraction and chemiluminescence detection, Lab on a Chip 6 (2006) 1387–1389.
[19] H. Chen, Q. Fang, X.-F. Yin, Z.-L. Fang, Microfluidic chip-based liquid–liquid extraction and preconcentration using a subnanoliter-droplet trapping technique, Lab on a Chip 5 (2005) 719–725.
[20] Z.-X. Cai, Q. Fang, H.-W. Chen, Z.-L. Fang, A microfluidic chip based liquid–liquid extraction system with microporous membrane, Analytica Chimica Acta 556 (2006) 151–156.
[21] A. Hibara, M. Tokeshi, K. Uchiyama, H. Hisamoto, T. Kitamori, Integrated multilayer flow system on a microchip, Analytical Sciences 17 (2001) 89–93.
[22] H. Miyaguchi, M. Tokeshi, Y. Kikutani, A. Hibara, H. Inoue, T. Kitamori, Microchip-based liquid–liquid extraction for gas-chromatography analysis of amphetamine-type stimulants in urine, Journal of Chromatography A 1129 (2006) 105–110.
[23] K. Sato, A. Hibara, M. Tokeshi, H. Hisamoto, T. Kitamori, Integration of chemical and biochemical analysis systems into a glass microchip, Analytical Sciences 19 (2003) 15–22.
[24] M. Tokeshi, T. Minagawa, T. Kitamori, Integration of a microextraction system: solvent extraction of a Co-2-nitroso-5-dimethylaminophenol complex on a microchip, Journal of Chromatography A 894 (2000) 19–23.
[25] M. Tokeshi, T. Minagawa, K. Uchiyama, A. Hibara, K. Sato, H. Hisamoto, T. Kitamori, Continuous-flow chemical processing on a microchip by combining microunit operations and a multiphase flow network, Analytical Chemistry 74 (2002) 1565–1571.
[26] A. Abou-Hassan, O. Sandre, V. Cabuil, Microfluidics in inorganic chemistry, Angewandte Chemie International Edition 49 (2010) 6268–6286.
[27] P. Mary, V. Studer, P. Tabeling, Microfluidic droplet-based liquid–liquid extraction, Analytical Chemistry 80 (2008) 2680–2687.

[28] X. Wang, C. Saridara, S. Mitra, Microfluidic supported liquid membrane extraction, Analytica Chimica Acta 543 (2005) 92–98.
[29] J. Jovanovic, E.V. Rebrov, T.A. Nijhuis, M.T. Kreutzer, V. Hessel, J.C. Schouten, Liquid–liquid flow in a capillary microreactor: hydrodynamic flow patterns and extraction performance, Industrial & Engineering Chemistry Research 51 (2012) 1015–1026.
[30] T. Maruyama, H. Matsushita, J.-i. Uchida, F. Kubota, N. Kamiya, M. Goto, Liquid membrane operations in a microfluidic device for selective separation of metal ions, Analytical Chemistry 76 (2004) 4495–4500.
[31] A. Berduque, J. O'Brien, J. Alderman, D.W.M. Arrigan, Microfluidic chip for electrochemically-modulated liquid–liquid extraction of ions, Electrochemistry Communications 10 (2008) 20–24.
[32] J. Berthier, V.-M. Tran, F. Mittler, N. Sarrut, The physics of a coflow microextractor: interface stability and optimal extraction length, Sensors and Actuators A: Physical 149 (2009) 56–64.
[33] A. Aota, K. Mawatari, T. Kitamori, Parallel multiphase microflows: fundamental physics, stabilization methods and applications, Lab on a Chip 9 (2009) 2470–2476.
[34] A. Aota, A. Hibara, T. Kitamori, Pressure balance at the liquid–liquid interface of micro countercurrent flows in microchips, Analytical Chemistry 79 (2007) 3919–3924.
[35] M. Tokeshi, T. Minagawa, T. Kitamori, Integration of a microextraction system on a glass chip: ion-pair solvent extraction of Fe(II) with 4,7-diphenyl-1,10-phenanthrolinedisulfonic acid and tri-n-octylmethylammonium chloride, Analytical Chemistry 72 (2000) 1711–1714.
[36] C. Priest, J. Zhou, R. Sedev, J. Ralston, A. Aota, K. Mawatari, T. Kitamori, Microfluidic extraction of copper from particle-laden solutions, International Journal of Mineral Processing 98 (2011) 168–173.
[37] V. Reddy, J.D. Zahn, Interfacial stabilization of organic-aqueous two-phase microflows for a miniaturized DNA extraction module, Journal of Colloid and Interface Science 286 (2005) 158–165.
[38] R. Seemann, M. Brinkmann, T. Pfohl, S. Herminghaus, Droplet based microfluidics, Reports on Progress in Physics 75 (2012) 41, 016601.
[39] S.-Y. Teh, R. Lin, L.-H. Hung, A.P. Lee, Droplet microfluidics, Lab on a Chip 8 (2008) 198–220.
[40] F. Scheiff, M. Mendorf, D. Agar, N. Reis, M. Mackley, The separation of immiscible liquid slugs within plastic microchannels using a metallic hydrophilic sidestream, Lab on a Chip 11 (2011) 1022–1029.
[41] H. Xiao, D. Liang, G. Liu, M. Guo, W. Xing, J. Cheng, Initial study of two-phase laminar flow extraction chip for sample preparation for gas chromatography, Lab on a Chip 6 (2006) 1067–1072.
[42] A. Hibara, S. Iwayama, S. Matsuoka, M. Ueno, Y. Kikutani, M. Tokeshi, T. Kitamori, Surface modification method of microchannels for gas–liquid two-phase flow in microchips, Analytical Chemistry 77 (2004) 943–947.
[43] M. Miyazaki, T. Honda, J. Kaneno, H. Nakamura, H. Maeda, Development of micro enzyme reactor for optical resolution, in: World Congress on Medical Physics and Biomedical Engineering 2006, 2007, pp. 238–241.
[44] J.G. Kralj, M.A. Schmidt, K.F. Jensen, Surfactant-enhanced liquid–liquid extraction in microfluidic channels with inline electric-field enhanced coalescence, Lab on a Chip 5 (2005) 531–535.
[45] S. Kuhn, R.L. Hartman, M. Sultana, K.D. Nagy, S. Marre, K.F. Jensen, Teflon-coated silicon microreactors: impact on segmented liquid–liquid multiphase flows, Langmuir 27 (2011) 6519–6527.
[46] C. Iliescu, H. Taylor, M. Avram, J. Miao, S. Franssila, A practical guide for the fabrication of microfluidic devices using glass and silicon, Biomicrofluidics 6 (2012) 016505–16516.
[47] K.F. Jensen, Silicon-based microchemical systems: characteristics and applications, MRS Bulletin 31 (2006) 101–107.
[48] P.N. Nge, C.I. Rogers, A.T. Woolley, Advances in microfluidic materials, functions, integration, and applications, Chemical Reviews 113 (2013) 2550–2583.
[49] D. Mark, S. Haeberle, G. Roth, F. von Stetten, R. Zengerle, Microfluidic lab-on-a-chip platforms: requirements, characteristics and applications, Chemical Society Reviews 39 (2010) 1153–1182.
[50] D. Bartolo, G. Degre, P. Nghe, V. Studer, Microfluidic stickers, Lab on a Chip 8 (2008) 274–279.
[51] C. Harrison, J. Cabral, T.C.M. Stafford, A. Karim, E.J. Amis, A rapid prototyping technique for the fabrication of solvent-resistant structures, Journal of Micromechanics and Microengineering 14 (2004) 153–158.
[52] L.H. Hung, R. Lin, A.P. Lee, Rapid microfabrication of solvent-resistant biocompatible microfluidic devices, Lab on a Chip 8 (2008) 983–987.
[53] A. Taberham, M. Kraft, M. Mowlem, H. Morgan, The fabrication of lab-on-chip devices from fluoropolymers, Journal of Micromechanics and Microengineering 18 (2008) 064011 (8 pp.).
[54] J.P. Rolland, E.C. Hagberg, G.M. Denison, K.R. Carter, J.M. De Simone, High-resolution soft lithography: enabling materials for nanotechnologies, Angewandte Chemie International Edition 43 (2004) 5796–5799.
[55] J.P. Rolland, R.M. Van Dam, D.A. Schorzman, S.R. Quake, J.M. DeSimone, Solvent-resistant photocurable "liquid teflon" for microfluidic device fabrication, Journal of the American Chemical Society 126 (2004) 2322–2323.
[56] T.J.A. Renckens, D. Janeliunas, H. van Vliet, J.H. van Esch, G. Mul, M.T. Kreutzer, Micromolding of solvent resistant microfluidic devices, Lab on a Chip 11 (2011) 2035–2038.
[57] N.S.G.K. Devaraju, M.A. Unger, Multilayer soft lithography of perfluoropolyether based elastomer for microfluidic device fabrication, Lab on a Chip 11 (2011) 1962–1967.
[58] K. Ren, W. Dai, J. Zhou, J. Su, H. Wu, Whole-teflon microfluidic chips, Proceedings of the National Academy of Sciences of the United States of America 108 (2011) 8162–8166.
[59] G.S. Fiorini, M. Yim, G.D.M. Jeffries, P.G. Schiro, S.A. Mutch, R.M. Lorenz, D.T. Chiu, Fabrication improvements for thermoset polyester (TPE) microfluidic devices, Lab on a Chip 7 (2007) 923–926.
[60] E. Roy, J.-C. Galas, T. Veres, Thermoplastic elastomers for microfluidics: towards a high-throughput fabrication method of multilayered microfluidic devices, Lab on a Chip 11 (2011) 3193–3196.
[61] J. Steigert, S. Haeberle, T. Brenner, C. Muller, C.P. Steinert, P. Koltay, N. Gottschlich, H. Reinecke, J. Ruhe, R. Zengerle, J. Ducree, Rapid prototyping of microfluidic chips in COC, Journal of Micromechanics and Microengineering 17 (2007) 333–341.
[62] G. Sharma, L. Klintberg, K. Hjort, Viton-based fluoroelastomer microfluidics, Journal of Micromechanics and Microengineering 21 (2011) 025016 (7 pp.).
[63] H. Sato, H. Matsumura, S. Keino, S. Shoji, An all SU-8 microfluidic chip with built-in 3D fine microstructures, Journal of Micromechanics and Microengineering 16 (2006) 2318–2322.
[64] H.-S. Noha, Y. Huangb, P.J. Hesketha, Parylene micromolding, a rapid and low-cost fabrication method for parylene microchannel, Sensors and Actuators B: Chemical 102 (2004) 78–85.
[65] S. Metz, R. Holzer, P. Renaud, Polyimide-based microfluidic devices, Lab on a Chip 1 (2001) 29–34.
[66] A. Asthana, Y. Asthana, I.-K. Sung, D.-P. Kim, Novel transparent poly(silazane) derived solvent-resistant, bio-compatible microchannels and substrates: application in microsystem technology, Lab on a Chip 6 (2006) 1200–1204.
[67] S. Begolo, G. Colas, J.-L. Viovy, L. Malaquin, New family of fluorinated polymer chips for droplet and organic solvent microfluidics, Lab on a Chip 11 (2011) 508–512.
[68] A. Hibara, M. Nonaka, H. Hisamoto, K. Uchiyama, Y. Kikutani, M. Tokeshi, T. Kitamori, Stabilization of liquid interface and control of two-phase confluence and separation in glass microchips by utilizing octadecylsilane modification of microchannels, Analytical Chemistry 74 (2002) 1724–1728.
[69] M. Miyazaki, Y. Yamaguchi, T. Honda, H. Maeda, Stable horizontal interface formation and separation of a water/oil flow by microfluidic reactor analyzed by direct observation and numerical simulation, The Open Chemical Engineering Journal 5 (2011) 13–17.
[70] J.S. Kuo, Y. Zhao, L. Ng, G.S. Yen, R.M. Lorenz, D.S. Lim, D.T. Chiu, Microfabricating high-aspect-ratio structures in polyurethane-methacrylate (PUMA) disposable microfluidic devices, Lab on a Chip 9 (2009) 1951–1956.
[71] Z.T. Cygan, J.o.T. Cabral, K.L. Beers, E.J. Amis, Microfluidic platform for the generation of organic-phase microreactors, Langmuir 21 (2005) 3629–3634.
[72] H. Gu, M.H.G. Duits, F. Mugele, A hybrid microfluidic chip with electrowetting functionality using ultraviolet (UV)-curable polymer, Lab on a Chip 10 (2010) 1550–1556.
[73] P. Wägli, A. Homsy, N.F. de Rooij, Norland optical adhesive (NOA81) microchannels with adjustable wetting behavior and high chemical resistance against a range of mid-infrared-transparent organic solvents, Sensors and Actuators B: Chemical 156 (2011) 0994–1001.
[74] A. Pohar, M. Lakner, I. Plazl, Parallel flow of immiscible liquids in a microreactor: modeling and experimental study, Microfluidics and Nanofluidics 12 (2012) 307–316.
[75] J.D. Law, K.N. Brewer, R.S. Herbst, T.A. Todd, D.J. Wood, Development and demonstration of solvent extraction processes for the separation of radionuclides from acidic radioactive waste, Waste Management 19 (1999) 27–37.
[76] J.D. Law, R.S. Herbst, T.A. Todd, V.N. Romanovskiy, V.A. Babain, V.M. Esimantovskiy, I.V. Smirnov, B.N. Zaitsev, The universal solvent extraction (UNEX) process. II. Flowsheet development and demonstration of the UNEX process for the separation of cesium, strontium, and actinides from actual acidic radioactive waste, Solvent Extraction and Ion Exchange 19 (2001) 23–36.
[77] V.N. Romanovskiy, I.V. Smirnov, V.A. Babain, T.A. Todd, R.S. Herbst, J.D. Law, K.N. Brewer, The universal solvent extraction (UNEX) process. I. Development of the UNEX process solvent for the separation of cesium, strontium, and the actinides from acidic radioactive waste, Solvent Extraction and Ion Exchange 19 (2001) 1–21.
[78] Y. Baba, M. Iwakuma, H. Nagami, Extraction mechanism for copper(II) with 2-hydroxy-4-n-octyloxybenzophenone oxime, Industrial & Engineering Chemistry Research 41 (2002) 5835–5841.

## Biographies

**Sachit Goyal** received his B.Tech. degree in Chemical Engineering from the Indian Institute of Technology (IIT), Delhi and M.S. degree in Chemical Engineering from the University of Illinois at Urbana Champaign. He is currently a PhD candidate at the University of Illinois at Urbana Champaign where his research focuses on the design and development of hybrid polymer-based microfluidic platforms for solid form screening of pharmaceutical parent compounds and for liquid–liquid extraction applications.

**Amit V. Desai** received his B.Tech. and M.Tech. degrees in Mechanical Engineering from the Indian Institute of Technology (IIT), Bombay, and his PhD degree in Mechanical and Nuclear Engineering from the Pennsylvania State University, University Park in the field of nanomechanics. He is currently a post-doctoral researcher in University of Illinois, Urbana-Champaign, where his research focuses on the

application of microfluidic technologies for life-sciences and biomedical applications, and development of electrostatic valves for integrated microfluidics.

**Robert W. Lewis** is a final year undergraduate student in Chemical Engineering at the University of Sheffield. As an exchange student during his third year at the University of Illinois, he worked on polymeric microreactors for liquid–liquid extraction.

**David R. Ranganathan** received his B.S. and M.S. degrees in Chemistry from the University of Madras, Chennai, and his PhD in Analytical Chemistry from the University of Camerino. He then joined the Reichert group at Washington University School of Medicine as a postdoctoral researcher focusing on the application of microfluidics toward radiopharmaceutical production.

**Hairong Li** received her B.S. and M.S. degrees from Nankai University and a PhD in Organic Chemistry from Louisiana State University. She then performed postdoctoral research at the University of Missouri, Columbia before joining the Reichert group at Washington University School of Medicine. Her research has focused on the development of novel peptide based imaging agents and the application of microfluidics in radiopharmaceutical production.

**Dexing Zeng** received his B.S. in Chemistry from the Harbin Engineering University and a PhD from the Technical Institute of Physics and Chemistry, Chinese Academy of Sciences. He then performed postdoctoral research at the University of Maryland's Biotechnology Institute before joining the Reichert group at Washington University School of Medicine as a postdoctoral researcher focusing on the application of microfluidics toward radiopharmaceutical production.

**David E. Reichert** received his PhD in Organic Chemistry from the University of Illinois at Urbana-Champaign. He then performed post-doctoral research at the Mallinckrodt Institute of Radiology at Washington University School of Medicine and is currently an Associate Professor of Radiology there. His research focuses on the use of computer-aided drug design directed toward radiopharmaceuticals, and in the development and application of microfluidics in radiopharmaceutical production.

**Paul J.A. Kenis** received his PhD in Chemical Engineering from Twente University, The Netherlands. After performing postdoctoral research at Harvard University he joined the faculty at the University of Illinois at Urbana-Champaign where he is currently a Professor and Head of the department of Chemical & Biomolecular Engineering, with affiliate appointments in the Beckman Institute, the Institute for Genomic Biology, the Frederick Seitz Material Research Laboratory, the Micro- & Nanotechnology Laboratory, and the departments of Bioengineering and Mechanical Science & Engineering. His research efforts include the development of microchemical systems: membraneless microfuel cells, microreactors (e.g., radiolabeling of biomolecules), microfluidic chips for pharmaceutical and membrane protein crystallization, platforms for biological cell studies (regenerative biology), sensors and valves for integrated microfluidic networks, and micro/nanofluidic tools for nanomanufacturing.